Springer Atmospheric Sciences

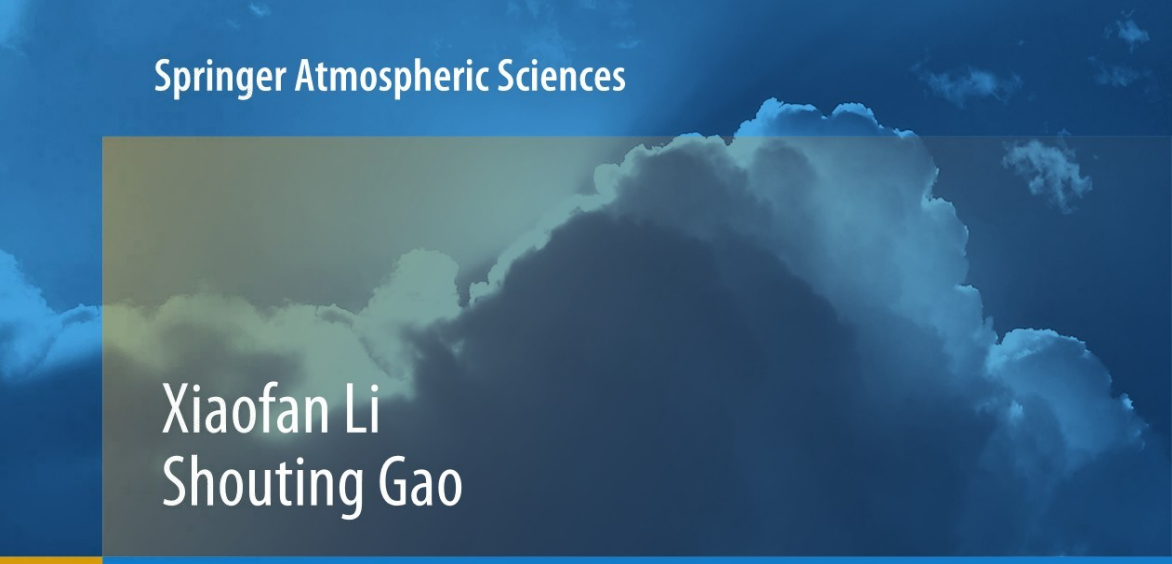

Xiaofan Li
Shouting Gao

Precipitation Modeling and Quantitative Analysis

Springer

Precipitation Modeling and Quantitative Analysis

Springer Atmospheric Sciences

For further volumes:
http://www.springer.com/series/10176

Xiaofan Li • Shouting Gao

Precipitation Modeling and Quantitative Analysis

Springer

Xiaofan Li
NOAA/NESDIS/Center for Satellite
Applications and Research
5200 Auth Road, Camp Springs,
MD 20746
USA
Xiaofan.Li@noaa.gov

Shouting Gao
Laboratory of Cloud-Precipitation
Physics and Severe Storms
Institute of Atmospheric Physics
Chinese Academy of Sciences
Chaoyang District, Beijing 100029
China
gst@mail.iap.ac.cn

ISBN 978-94-007-2380-1 e-ISBN 978-94-007-2381-8
DOI 10.1007/978-94-007-2381-8
Springer Dordrecht Heidelberg London New York

Library of Congress Control Number: 2011941660

To my wife Qin for her encouragement and support

Xiaofan Li

To my wife Rongyu for her patience and support

Shouting Gao

Foreword

Precipitation is interlinked with atmospheric dynamics and thermodynamics through the latent heat released during phase changes of water, and the heat absorbed during the evaporation of precipitation. The nonlinear relationships involved with precipitation processes coupled to atmospheric dynamics are major sources of uncertainty for all prediction models. Floods caused by torrential rainfall, along with weather hazards, cause enormous economic loss and affect livelihood around the world. Understanding precipitation processes and how these interact with dynamics is a vital step towards improving the skill of prediction models. This will help day-to-day planning by individuals, longer-term decision making by institutions and governments, and foster an improved relationship between science and society.

Improving our knowledge of precipitation processes requires the formulation of quantitative relationships between microphysics, clouds, water vapor, latent heating and dynamics. During the past 7 years, along with their research groups, Professor Shouting Gao of the Institute of Atmospheric Physics in Beijing, China and Dr.Xiaofan Li of NOAA's National Environmental Satellite, Data, and Information Service (NESDIS) have made considerable progress with precipitation modeling. In number of publications they have derived diagnostic equations involving clouds, water vapor and energy. They applied these equations to enhance our understanding how water, atmospheric dynamics, cloud processes interact in precipitation systems.

This well-written book by Dr. Xiaofan Li and Professor Shouting Gao updates and reviews precipitation modeling and quantitative analysis through the effects of physical processes. Their approach is focused on two-dimensional precipitation modeling of selected periods during the Tropical Ocean Global Atmosphere Coupled Ocean-Atmosphere Response Experiment (TOGA COARE), the landfall of severe tropical storm Bilis (2006), and pre-summer rainfall over southern China in 2008. This includes the validation of numerical models against observations. They provide detailed derivations of the salient equations, along with quantitative analyses of the effects of sea-surface temperature, vertical wind shear, cloud-radiation interaction, and ice clouds on heavy rainfall. They evaluate the sensitivity of the numerical models to uncertainties in the initial conditions, and describe basic concepts such as precipitation efficiency.

The authors provide a solid foundation for the quantitative analysis of precipitation processes and lay a basis for future three-dimensional precipitation modeling pertinent to weather and climate.

Senior Scientist Mitchell Moncrieff
National Center for Atmospheric Research

Introduction

Precipitation is one of the most important quantities in meteorology and hydrology. Because floods resulting from torrential rainfall associated with severe weathers and storms can cause tremendous economic loss, the accurate measurement and the quantitative estimate and forecast of precipitation have significant economic and social implications in rainfall-rich countries. However, accurate estimate of surface rain rate is difficult due to the fact that precipitation processes are nonlinearly associated with the dynamic, thermodynamic, cloud microphysical and radiative processes. While many previous studies have contributed to the qualitative analysis of precipitation processes, quantitative analysis of precipitation processes has seldom been conducted simply because diagnostic precipitation equations associated with heat and water vapor processes have not been available. Facing this challenge, in 2005, the authors combined water vapor and cloud budget to derive a water-vapor-related diagnostic precipitation equation for quantitatively identifying dominant water vapor and cloud processes associated with precipitation. In 2010, the authors combined heat and cloud budgets to derive a thermal-related precipitation equation for quantitatively identifying dominant thermal and cloud processes associated with precipitation. This set of precipitation equations has been widely used to study the effects of sea surface temperature (SST), vertical wind shear, radiation, and ice clouds on torrential rainfall and diurnal cycle, precipitation efficiency; the sensitivity of precipitation modeling to the uncertainty of initial conditions; and to develop a new rainfall partitioning scheme.

The material in this book is based on our research work in the last 7 years. This book starts with precipitation modeling with the two-dimensional version of the Goddard Cumulus Ensemble Model and an evaluation of modeling with available observations. The book details the derivation of precipitation equations and covers many research aspects on the effects of sea surface temperature, vertical wind shear, radiation, and ice clouds on rainfall in idealized cases without large-scale vertical velocity, in a tropical rainfall case during the Tropical Ocean Global Atmosphere Coupled Ocean-Atmosphere Response Experiment (TOGA COARE), and in torrential rainfall cases associated with severe tropical storm Bilis (2006) and a pre-summer rainfall event over southern China in 2008. The material in this book has

been used in part of a graduate course at the Graduate School, Chinese Academy of Sciences, Beijing, China. Therefore, this book can be used as both reference and as a textbook for graduate students, researchers, operational forecasters and those whose research interests include precipitation modeling, analysis, and forecasts.

This book is comprised of nine chapters. Chap. 1 presents and evaluates precipitation modeling with available observations. Chap. 2 gives detailed derivations of a set of precipitation equations and their applications to the analysis of precipitation processes in idealized rainfall cases and torrential rainfall cases in Bilis and pre-summer rainfall events. Chap. 3 discusses tropical rainfall processes during TOGA COARE. The effects of SST, vertical wind shear, ice clouds, and cloud radiative processes on the development of rainfall are respectively discussed in Chaps. 4–7. Precipitation efficiency is analyzed in Chap. 8, and the sensitivity of precipitation modeling to uncertainty of initial conditions is studied in Chap. 9.

We would like to thank Dr. Mitchell W. Moncrieff, the senior scientist of the National Corporation for Atmospheric Research who read the book draft and wrote the preface for this book. Our sincere thanks also go to Dr. Wei-Kuo Tao at NASA/Goddard Space Flight Center (GSFC), Professor Ming-Dah Chou at National Taiwan University, and Professor Minghua Zhang at the State University of New York, Stony Brook for providing the two-dimensional Goddard Cumulus Ensemble (GCE) model, the radiative transfer code used in GCE model, and TOGA COARE forcing data, respectively. We also thank Dr. Hsiao-Ming Hsu at the National Center for Atmospheric Research and Prof. Xiaoqing Wu at the Iowa State University for their comments, Drs. Fan Ping, Xiaopeng Cui, and Yushu Zhou at the Institute of Atmospheric Physics, Chinese Academy of Sciences, Dr. Donghai Wang at the China Meteorological Administration, Prof. Xinyong Shen at the Nanjing University of Information Science and Technology, Dr. Jian-Jian Wang at the Goddard Center for Earth Science and Technology, University of Maryland, Baltimore County, and Mr. Yi Wang at the Jiangsu Weather Bureau for efficient and productive research collaborations, and Miss Di Li at the University of Pennsylvania Law School, Philadelphia for editing this book.

We are also indebted to Dr. Robert K. Doe of Springer for his editorial efforts.

This work was supported by the National Key Basic Research and Development Project of China No.2009CB421505, the National Natural Sciences Foundation of China under the Grant No.40930950 and 41075043.

Camp Springs, Maryland, USA — Xiaofan Li
Beijing, China — Shouting Gao

Contents

1 Cloud-Resolving Modeling of Precipitation 1
1.1 Cloud-Resolving Model 2
1.2 Weather Events and Large-Scale Forcing for Precipitation Modeling 6
1.2.1 Experiment COARE 6
1.2.2 Experiment SCSMEX 6
1.2.3 Experiment BILIS 8
1.2.4 Experiment PSR 9
1.3 Comparison Between Simulations and Observations 9
1.3.1 Temperature and Specific Humidity 9
1.3.2 Surface Rain Rate 12
1.3.3 Reflectivity 15
1.4 Equilibrium Simulations with Zero Large-Scale Vertical Velocity 20
1.5 Comparison Between 2D and 3D Model Simulations 22
References 23

2 Precipitation Equations and Process Analysis 27
2.1 Precipitation Equations 27
2.2 Equilibrium Model Simulation with Zero Large-Scale Vertical Velocity 32
2.2.1 Time-Mean Analysis 32
2.2.2 Analysis of Diurnal Variation 35
2.3 Simulation of Rainfall Event During SCSMEX 38
2.4 Simulation of Torrential Rainfall Event During the Landfall of Severe Tropical Storm Bilis (2006) 40
2.5 Simulation of Pre-summer Heavy Rainfall Event over Southern China in June 2008 58
References 60

3 Tropical Precipitation Processes 63
3.1 Model Domain Mean Analysis 63
3.1.1 Effects of Mean Hydrometeor Loss/Gain on Mean Rainfall in the Presence of Mean Water Vapor Convergence and Mean Local Atmospheric Drying 64
3.1.2 Effects of Mean Local Atmospheric Drying/Moistening on Mean Rainfall 71
3.1.3 Effects of Mean Local Atmospheric Drying/Moistening and Mean Hydrometeor Loss/Gain on Mean Rainfall in the Presence of the Mean Water Vapor Divergence 73
3.2 Grid-Scale Analysis 74
3.3 Tropical Rainfall Responses to the Large-Scale Forcing 82
3.4 Effects of Time-Dependent Large-Scale Forcing, Solar Zenith Angle, and Sea Surface Temperature on Time-Mean Tropical Rainfall Processes 92
3.5 Diurnal Cycle 101
References 108

4 Effects of Sea Surface Temperature 111
4.1 Introduction 111
4.2 Time-Mean Analysis 111
4.3 Analysis of Diurnal Variation 116
References 124

5 Effects of Vertical Wind Shear 125
5.1 Introduction 125
5.2 Effects of Vertical Wind Shear on Severe Tropical Storm Rainfall 126
5.3 Effects of Vertical Wind Shear on Pre-summer Heavy Rainfall 133
References 136

6 Microphysical and Radiative Effects of Ice Clouds 137
6.1 Introduction 137
6.2 Effects of Ice Clouds on Rainfall in the Simulations with Zero Large-Scale Vertical Velocity 139
6.2.1 Time-Mean Analysis 139
6.2.2 Diurnal Analysis 141
6.2.3 Vertical Structures of Thermal and Water Vapor Budgets 150
6.3 Effects of Ice Clouds on Severe Tropical Storm Rainfall 159
6.4 Effects of Ice Clouds on Pre-summer Heavy Rainfall 166
References 172

7 Cloud Radiative Effects 175
7.1 Introduction 175
7.2 Radiative Effects of Water Clouds on Rainfall in the Simulations with Zero Large-Scale Vertical Velocity 176
7.2.1 Time-Mean Analysis 176
7.2.2 Analysis of Diurnal Variation 178

7.3 Effects of Cloud Radiative Process and Cloud-Radiation Interaction on Severe Tropical Storm Rainfall 187
7.4 Cloud Radiative Effects on Pre-summer Heavy Rainfall 199
7.4.1 Cloud Radiative Effects 199
7.4.2 Radiative Effects of Water Clouds 201
References 206

8 Precipitation Efficiency 209
References 218

9 Sensitivity of Precipitation Modeling to Uncertainty of Initial Conditions 219
9.1 Introduction 219
9.2 Sensitivity of Precipitation Modeling to Uncertainty of Initial Conditions of Temperature, Water Vapor, and Clouds 220
9.3 Sensitivity of Precipitation Modeling to Uncertainty of Vertical Structures of Initial Conditions 225
References 234

Index 237

Abbreviations and Acronyms

2D	Two-dimensional
3D	Three-dimensional
AIRS	Atmospheric Infrared Sounder
AMSU	Advanced Microwave Sounding Unit
ARM	Atmospheric Radiation Measurement
CAPE	Convective available potential energy
CFAD	Contoured frequency with altitude diagram
COARE	Coupled Ocean-Atmosphere Response Experiment
CMPE	Cloud-microphysics precipitation efficiency
EQ	Equator
GCE	Goddard cumulus ensemble
GDAS	Global Data Assimilation System
GSFC	Goddard Space Flight Center
HSB	Humidity Sounder for Brazil
IFA	Intensive Flux Array
IMET	Improved Meteorological
IOP	Intensive Observing Period
IR	Infrared
IWP	Ice Water Path
LFC	Level of free convection
LSPE	Large-scale precipitation efficiency
LST	Local standard time
LWP	Liquid Water Path
MSPPS	Microwave Surface and Precipitation Products System
NASA	National Aeronautics and Space Administration
NCEP	National Centers for Environmental Prediction

NESDIS	National Environmental Satellite, Data, and Information Service
NOAA	National Oceanic and Atmospheric Administration
PSU	Practical salinity units
PV	Potential vorticity
PW	Precipitable water
RMPE	Rain Microphysics Precipitation Efficiency
RMS	Root-mean-square
SCSMEX	South China Sea Monsoon Experiment
SST	Sea surface temperature
TOGA	Tropical Ocean Global Atmosphere
TMI	TRMM Microwave Imager
TRMM	Tropical Rainfall Measuring Mission

Chapter 1
Cloud-Resolving Modeling of Precipitation

Precipitation has important impacts on people's daily life and torrential precipitation could bring tremendous losses in economy and cause fatalities. Thus, precipitation always is one of the top priorities in operational forecast and scientific research. Precipitation is a result of convective development under a favorable environment. The unstable energy is accumulated with favorable environmental thermodynamic conditions when the clouds and associated precipitation are absent. The release of unstable energy drives the growth of clouds that eventually leads to precipitation. The development of clouds and precipitation has important feedback to the environment by redistributing temperature, water vapor, and momentum via radiative, cloud microphysical and dynamic processes. The precipitation processes are determined by environment thermal and water vapor conditions through cloud microphysical processes. The analysis of thermal, water vapor, and cloud microphysical budgets will enhance understanding of precipitation, which is beneficial to the improvement of quantitative precipitation forecast. However, important information such as cloud microphysical processes is not conventionally available, which make observational analysis rather difficult.

The cloud-resolving models provide a practical tool for process studies associated with surface rainfall processes (e.g., Gao and Li 2008a). The model has fine horizontal resolution to simulate individual cloud and includes radiative and prognostic cloud microphysical schemes to simulate cloud-radiation interaction processes (Sect. 1.1). In this chapter, two-dimensional (2D) cloud-resolving model simulations of tropical convective events during the Tropical Ocean Global Atmosphere Coupled Ocean–atmosphere Response Experiment (TOGA COARE) (Experiment COARE; Gao and Li 2008b) and South China Sea Monsoon Experiment (SCSMEX) (Experiment SCSMEX; Wang et al. 2007), torrential rainfall event during the landfall of severe tropical storm Bilis (2006) (Experiment BILIS; Wang et al. 2009), and pre-summer heavy rainfall event over southern China in June 2008 (Experiment PSR; Wang et al. 2010; Shen et al. 2011) will be discussed in terms of large-scale forcing (Sect. 1.2), temperature, specific humidity, surface rain rate, reflectivity, and cloud hydrometeor mixing ratios (Sect. 1.3). Equilibrium simulations with zero large-scale vertical

X. Li and S. Gao, *Precipitation Modeling and Quantitative Analysis*,
Springer Atmospheric Sciences, DOI 10.1007/978-94-007-2381-8_1,

velocity are introduced in Sect. 1.4. Comparisons between 2D and three-dimensional (3D) simulations are discussed in Sect. 1.5.

1.1 Cloud-Resolving Model

The cloud-resolving model was originally developed by Soong and Ogura (1980); Soong and Tao (1980) for studying convection at the timescale of shorter than a day. This model was significantly improved by Tao and Simpson (1993) at the National Aeronautics and Space Administration (NASA) Goddard Space Flight Center (GSFC) and was modified by Sui et al. (1994, 1998) for studying tropical convection and associated hydrological cycles at the timescale from weeks to months and tropical equilibrium states. The model was named the Goddard cumulus ensemble (GCE) model. The model includes prognostic equations for perturbation zonal (u) and vertical (w) winds, potential temperature (θ), specific humidity (q_v), and five cloud hydrometeor mixing ratios. The 2D non-hydrostatic governing equations with anelastic approximation can be expressed by

$$\frac{\partial u'}{\partial x}+\frac{1}{\overline{\rho}}\frac{\partial(\overline{\rho}w')}{\partial z}=0, \tag{1.1a}$$

$$\frac{\partial u'}{\partial t}=-\frac{\partial}{\partial x}(2u'\overline{u}^{o}+u'u')-\frac{1}{\overline{\rho}}\frac{\partial}{\partial z}\overline{\rho}(w'\overline{u}^{o}+\overline{w}^{o}u'+w'u'-\overline{w'u'})$$
$$-c_p\frac{\partial(\overline{\theta}\pi')}{\partial x}+D_u-\overline{D}_u, \tag{1.1b}$$

$$\frac{\partial w'}{\partial t}=-\frac{\partial}{\partial x}(u'\overline{w}^{o}+\overline{u}^{o}w'+u'w')-\frac{1}{\overline{\rho}}\frac{\partial}{\partial z}\overline{\rho}(2w'\overline{w}^{o}+w'w'-\overline{w'w'})$$
$$-c_p\frac{\partial(\overline{\theta}\pi')}{\partial z}+g\left(\frac{\theta'}{\theta_o}+0.61q_v'-q_l'\right)+D_w-\overline{D}_w, \tag{1.1c}$$

$$\frac{\partial\theta}{\partial t}=-\frac{\partial(u'\theta')}{\partial x}-\overline{u}^{o}\frac{\partial\theta'}{\partial x}-\frac{1}{\overline{\rho}}\frac{\partial}{\partial z}(\overline{\rho}w'\theta')-\overline{w}^{o}\frac{\partial\theta'}{\partial z}-w'\frac{\partial\overline{\theta}}{\partial z}$$
$$+\frac{Q_{cn}}{\pi c_p}+\frac{Q_R}{\pi c_p}-\overline{u}^{o}\frac{\partial\overline{\theta}^{o}}{\partial x}-\overline{w}^{o}\frac{\partial\overline{\theta}}{\partial z}+D_\theta, \tag{1.1d}$$

$$\frac{\partial q_v}{\partial t}=-\frac{\partial(u'q_v')}{\partial x}-\overline{u}^{o}\frac{\partial q_v'}{\partial x}-\overline{w}^{o}\frac{\partial q_v'}{\partial z}-w'\frac{\partial\overline{q}_v}{\partial z}-\frac{1}{\overline{\rho}}\frac{\partial}{\partial z}\overline{\rho}w'q_v'$$
$$-S_{qv}-\overline{u}^{o}\frac{\partial q_v'}{\partial x}-\overline{w}^{o}\frac{\partial\overline{q}_v}{\partial z}+D_{qv}, \tag{1.1e}$$

$$\frac{\partial q_c}{\partial t} = -\frac{\partial (uq_c)}{\partial x} - \frac{1}{\overline{\rho}} \frac{\partial (\overline{\rho} w q_c)}{\partial z} + S_{qc} + D_{qc}, \tag{1.1f}$$

$$\frac{\partial q_r}{\partial t} = -\frac{\partial (uq_r)}{\partial x} - \frac{1}{\overline{\rho}} \frac{\partial}{\partial z} \overline{\rho}(w - w_{Tr}) q_r + S_{qr} + D_{qr}, \tag{1.1g}$$

$$\frac{\partial q_i}{\partial t} = -\frac{\partial (uq_i)}{\partial x} - \frac{1}{\overline{\rho}} \frac{\partial (\overline{\rho} w q_i)}{\partial z} + S_{qi} + D_{qi}, \tag{1.1h}$$

$$\frac{\partial q_s}{\partial t} = -\frac{\partial (uq_s)}{\partial x} - \frac{1}{\overline{\rho}} \frac{\partial}{\partial z} \overline{\rho}(w - w_{Ts}) q_s + S_{qs} + D_{qs}, \tag{1.1i}$$

$$\frac{\partial q_g}{\partial t} = -\frac{\partial (uq_g)}{\partial x} - \frac{1}{\overline{\rho}} \frac{\partial}{\partial z} \overline{\rho}(w - w_{Tg}) q_g + S_{qg} + D_{qg}, \tag{1.1j}$$

where

$$Q_{cn} = \sum_{I=1}^{20} CNP_I, \tag{1.2a}$$

$$S_{qv} = \sum_{I=1}^{7} P_I, \tag{1.2b}$$

$$S_{qc} = \sum_{I=1}^{9} CWP_I, \tag{1.2c}$$

$$S_{qr} = \sum_{I=1}^{12} RP_I, \tag{1.2d}$$

$$S_{qi} = \sum_{I=1}^{9} CIP_I, \tag{1.2e}$$

$$S_{qs} = \sum_{I=1}^{15} SP_I, \tag{1.2f}$$

$$S_{qg} = \sum_{I=1}^{14} GP_I, \tag{1.2g}$$

$$\begin{aligned} CNP_I = {} & (L_v P_{CND} - L_v P_{REVP}), L_s P_{DEP}, L_s (1-\delta_1) P_{SDEP} (T < T_o), \\ & L_s (1-\delta_1) P_{GDEP} (T < T_o), -L_s P_{MLTS} (T > T_o), -L_s P_{MLTG} (T > T_o), \\ & L_f P_{SACW} (T < T_o), L_f P_{SFW} (T < T_o), L_f P_{GACW} (T < T_o), \\ & L_f P_{IACR} (T < T_o), L_f P_{GACR} (T < T_o), L_f P_{SACR} (T < T_o), \\ & L_f P_{GFR} (T < T_o), -L_f P_{RACS} (T > T_o), -L_f P_{SMLT} (T > T_o), \\ & -L_f P_{GMLT} (T > T_o), L_f P_{IHOM} (T < T_{oo}) - L_f P_{IMLT} (T > T_o), \\ & L_f P_{IDW} (T_{oo} < T < T_o)), \end{aligned} \tag{1.2h}$$

$$P_I = (P_{CND},\ P_{DEP},\ (1-\delta_1)\ P_{SDEP}\ (T<T_o),(1-\delta_1)\,P_{GDEP}\ (T<T_o),\\ -P_{REVP},-P_{MLTG},-P_{MLTS}), \tag{1.2i}$$

$$CWP_I = (-P_{SACW},-P_{RAUT},-P_{RACW},-P_{SFW}\ (T<T_o),-P_{GACW},\\ P_{CND},-P_{IHOM}\ (T<T_{oo}),P_{IMLT}\ (T>T_o),\\ -P_{IDW}\ (T_{oo}<T<T_o)), \tag{1.2j}$$

$$RP_I = (P_{SACW}\ (T>T_o),P_{RAUT},P_{RACW},P_{GACW}\ (T>T_o),\\ -P_{REVP},P_{RACS}\ (T>T_o),-P_{IACR}\ (T<T_o),-P_{GACR}\ (T<T_o),\\ -P_{SACR}\ (T<T_o),-P_{GFR}\ (T<T_o),P_{SMLT}\ (T>T_o),\\ P_{GMLT}\ (T>T_o)), \tag{1.2k}$$

$$CIP_I = (-P_{SAUT}\ (T<T_o),-P_{SACI}\ (T<T_o),-P_{RACI}\ (T<T_o),\\ -P_{SFI}\ (T<T_o),-P_{GACI}\ (T<T_o),P_{IHOM}\ (T<T_{oo}),\\ -P_{IMLT}\ (T>T_o),P_{IDW}\ (T_{oo}<T<T_o,P_{DEP})), \tag{1.2l}$$

$$SP_I = (P_{SAUT}\ (T<T_o),P_{SACI}\ (T<T_o),P_{SACW}\ (T<T_o),\\ P_{SFW}\ (T<T_o),P_{SFI}\ (T<T_o),P_{RACI}\ (T<T_o),\\ -P_{RACS}\ (T>T_o),-P_{GACS},-P_{SMLT}\ (T>T_o),\\ -P_{RACS}\ (T<T_o),P_{SACR}\ (T<T_o),P_{SDEP}\ (T<T_o),-P_{MLTS}\ (T>T_o),\\ P_{IACR}\ (T<T_o),-P_{WACS}\ (T<T_o)), \tag{1.2m}$$

$$GP_I = (P_{RACI}\ (T<T_o),P_{GACI}\ (T<T_o),\\ P_{GACW}\ (T<T_o),P_{SACW}\ (T<T_o),P_{GACS},\\ P_{IACR}\ (T<T_o),P_{GACR}\ (T<T_o),P_{RACS}\ (T<T_o),P_{GFR}\ (T<T_o),\\ P_{WACS}\ (T<T_o),-P_{GMLT}\ (T>T_o),P_{GDEP}\ (T<T_o),-P_{MLTG}\ (T>T_o),\\ P_{SACR}\ (T<T_o)). \tag{1.2n}$$

and

$$\delta_1 = 1,\ \text{only if}\ q_c + q_i > 10^{-8}\ gg^{-1}, T<T_o, \tag{1.2o}$$

$$\delta_2 = 1,\ \text{only if}\ q_s + q_r < 10^{-4}\ gg^{-1}, T<T_o, \tag{1.2p}$$

$$\delta_3 = 1,\ \text{only if}\ q_r > 10^{-4}\ gg^{-1}, T<T_o, \tag{1.2q}$$

$$\delta_4 = 1,\ \text{only if}\ q_s \le 10^{-4}\ gg^{-1}, q_c > 5\times10^{-4}\ gg^{-1}, T<T_o \tag{1.2r}$$

Here, q_c, q_r, q_i, q_s, and q_g, are the mixing ratios of cloud water, raindrops, cloud ice, snow, and graupel, respectively; $\pi=(p/p_0)^{\kappa}$, $\kappa=R/c_p$; R is the gas constant; c_p is the specific heat of dry air at constant pressure p, and p_o = 1,000 hPa; T is air temperature, and T_o = 0°C, T_{oo} = −35°C. L_v, L_s, and L_f are latent heat of vaporization, sublimation,

Table 1.1 List of microphysical processes and their parameterization schemes

Notation	Description	Scheme
P_{MLTG}	Growth of vapor by evaporation of liquid from graupel surface	RH84
P_{MLTS}	Growth of vapor by evaporation of melting snow	RH83
P_{REVP}	Growth of vapor by evaporation of raindrops	RH83
P_{IMLT}	Growth of cloud water by melting of cloud ice	RH83
P_{CND}	Growth of cloud water by condensation of supersaturated vapor	TSM
P_{GMLT}	Growth of raindrops by melting of graupel	RH84
P_{SMLT}	Growth of raindrops by melting of snow	RH83
P_{RACI}	Growth of raindrops by the accretion of cloud ice	RH84
P_{RACW}	Growth of raindrops by the collection of cloud water	RH83
P_{RACS}	Growth of raindrops by the accretion of snow	RH84
P_{RAUT}	Growth of raindrops by the autoconversion of cloud water	LFO
P_{IDW}	Growth of cloud ice by the deposition of cloud water	KFLC
P_{IACR}	Growth of cloud ice by the accretion of rain	RH84
P_{IHOM}	Growth of cloud ice by the homogeneous freezing of cloud water	
P_{DEP}	Growth of cloud ice by the deposition of supersaturated vapor	TSM
P_{SAUT}	Growth of snow by the conversion of cloud ice	RH83
P_{SACI}	Growth of snow by the collection of cloud ice	RH83
P_{SACW}	Growth of snow by the accretion of cloud water	RH83
P_{SFW}	Growth of snow by the deposition of cloud water	KFLC
P_{SFI}	Depositional growth of snow from cloud ice	KFLC
P_{SACR}	Growth of snow by the accretion of raindrops	LFO
P_{SDEP}	Growth of snow by the deposition of vapor	RH83
P_{GACI}	Growth of graupel by the collection of cloud ice	RH84
P_{GACR}	Growth of graupel by the accretion of raindrops	RH84
P_{GACS}	Growth of graupel by the accretion of snow	RH84
P_{GACW}	Growth of graupel by the accretion of cloud water	RH84
P_{WACS}	Growth of graupel by the riming of snow	RH84
P_{GDEP}	Growth of graupel by the deposition of vapor	RH84
P_{GFR}	Growth of graupel by the freezing of raindrops	LFO

The schemes are Lin et al. (1983, LFO), Rutledge and Hobbs (1983, 1984, RH83, RH84); Tao et al. (1989, TSM), and Krueger et al. (1995, KFLC)

and fusion at 0°C, respectively, and $L_s = L_v + L_f$. Q_R in (1.1d) is the radiative heating rate due to convergence of the net flux of solar and infrared radiative fluxes calculated by solar and thermal infrared radiation parameterization schemes (Chou et al. 1991, 1998; Chou and Suarez 1994). The cloud microphysical terms in prognostic cloud Eqs. 1.2h–1.2n are calculated by single-moment cloud microphysical parameterization schemes (Lin et al. 1983; Rutledge and Hobbs 1983, 1984; Tao et al. 1989; Krueger et al. 1995), which are defined in Table 1.1. w_{Tr} in (1.1g), w_{Ts} in (1.1i) and w_{Tg} in (1.1j) are terminal velocities for raindrops, snow, and graupel, respectively; overbar denotes a model domain mean; prime is a perturbation from model domain mean; and superscript ^{o} is an imposed observed value. The model uses cyclic lateral boundaries and has a horizontal domain of 768 km with 33 vertical levels, and its horizontal and temporal resolutions are 1.5 km and 12 s, respectively. The top

model level is 42 hPa. The vertical grid resolution ranges from about 40–200 m near the surface to about 1 km near 100 hPa. The observed surface temperature and specific humidity over land and the observed sea surface temperature over ocean are uniformly imposed on each model grid to calculate surface sensible heat flux and evaporation flux. The model details can be found in Gao and Li (2008a).

1.2 Weather Events and Large-Scale Forcing for Precipitation Modeling

1.2.1 Experiment COARE

The cloud resolving model in experiment COARE is forced by large-scale vertical velocity, zonal wind, and horizontal advections derived using 6-hourly TOGA COARE observations within the Intensive Flux Array (IFA) region from Professor M. Zhang of the State University of New York at Stony brook and hourly SST at the Improved Meteorological (IMET) surface mooring buoy (1.75°S, 156°E) from Weller and Anderson (1996), (Gao and Li 2008b). The model is integrated from 0400 Local Standard Time (LST) 22 December 1992 to 0400 LST 08 January 1993. Figure 1.1 shows the time-height cross sections of the large-scale vertical velocity, zonal wind, and the time series of SST from 0400 LST 22 December 1992 to 0400 LST 8 January 1993, which are imposed in the model. On 22–27 December 1992, the strong upward motions with a maximum of 8 cm s^{-1} are associated with westerly winds of 10 m s^{-1}. From 28 December 1992 to 2 January 1993, the downward motions of −1 cm s^{-1} occur while the westerly winds reach a maximum of 16 m s^{-1}. In the last few days, the moderate upward motions occur as westerly winds weaken. Except for the last 4 days, the SST has only a weak diurnal variation with a slowly decreasing trend.

1.2.2 Experiment SCSMEX

The forcing (Fig. 1.2) averaged over the area of 16°–23°N, 116°–117°E using 6-hourly observational data from SCSMEX Intensive Observing Period (Johnson and Ciesielski 2002) and daily-mean SST data (not shown) retrieved from NASA/Tropical Rainfall Measuring Mission (TRMM) Microwave Imager (TMI) radiometer with a 10.7 GHz channel (Wentz et al. 2000) are imposed in the model in Experiment SCSMEX (Wang et al. 2007). The model is integrated from 0200 LST 20 May to 1400 LST 24 May 1998. Downward motions occur in early morning of 20 May 1998, followed by the strong upward motions around early afternoon of 20 May. The upward motions continue to dominate the rest of the integration period, while they are briefly interrupted by a few downward motion events, in particular, in the mid and lower troposphere. The southerly winds start to diminish with the strengthened

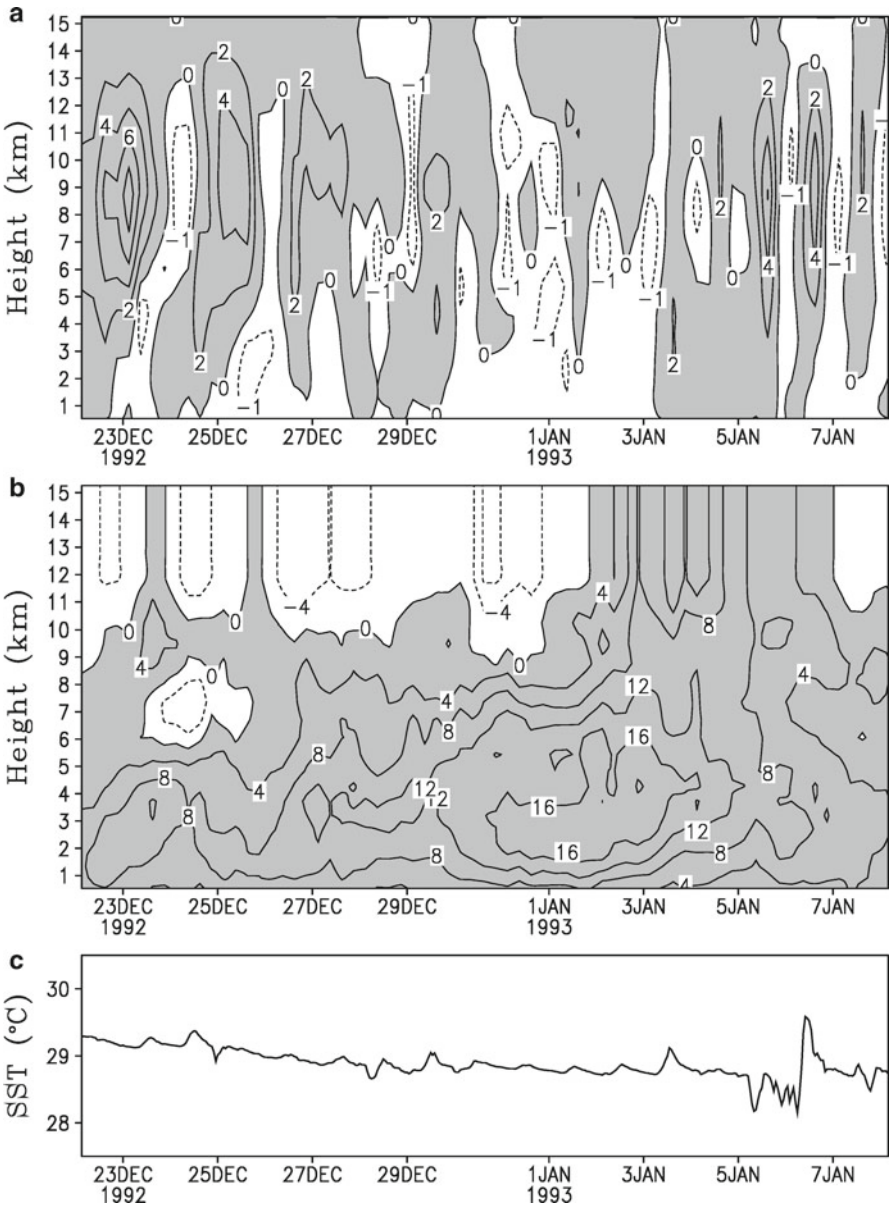

Fig. 1.1 Time-height distributions of (**a**) vertical velocity (cm s^{-1}) and (**b**) zonal wind (m s^{-1}), and (**c**) time series of sea surface temperature (°C) observed and derived from TOGA COARE, which are used in Experiment COARE as the large-scale forcing. Upward motion in (**a**) and westerly wind in (**b**) are *shaded* (After Gao and Li 2008b)

northerly winds, which propagate downward. The southerly winds regain strengths in the mid and lower troposphere on the last day of the integration period, although the northerly winds remain strong in the upper troposphere.

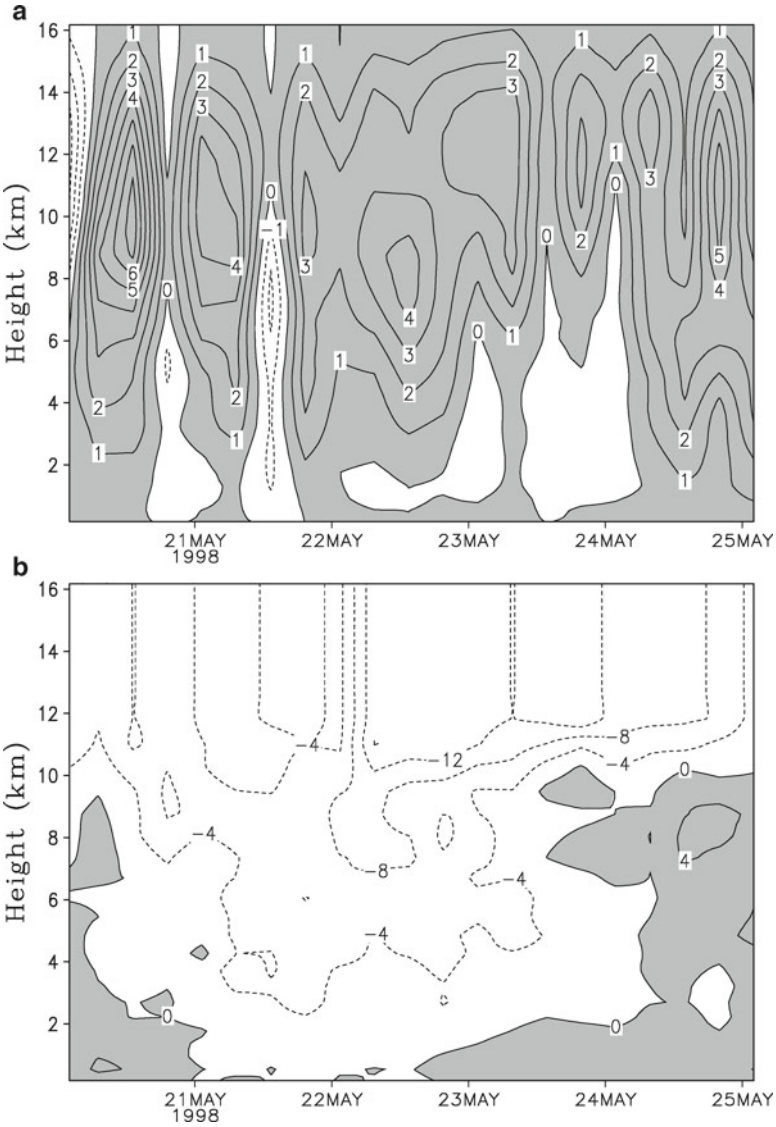

Fig. 1.2 Temporal and vertical distributions of (**a**) vertical velocity (cm s^{-1}) and (**b**) meridional wind (m s^{-1}) during selected SCSMEX period, which are used in Experiment SCSMEX as the large-scale forcing. Upward motion in (**a**) and southerly wind in (**b**) are *shaded*. The *arrows* above (**a**) indicate the analysis period in this study (After Wang et al. 2007)

1.2.3 Experiment BILIS

The reanalysis data from National Centers for Environmental Prediction (NCEP)/ Global Data Assimilation System (GDAS) that have a horizontal resolution of $1° \times 1°$

and a temporal resolution of four times per day are used to construct large-scale forcing (vertical velocity, zonal wind, and horizontal temperature and vapor advection) in Experiment BILIS (Wang et al. 2009). Bilis made its second landfall in Fujian, China early on July 14, and then weakened into a tropical depression over land the next day. It brought a torrential rainfall over the areas of southeast China (Fujian, Guangdong, Guangsi, and Hunan provinces) during 15–17 July 2006, and dissipated on 18 July 2006. The model is integrated from 0800 LST 14 July to 0800 LST 20 July 2006 with the forcing averaged in a rectangular box of 108–116°E, 23–24°N (Fig. 1.3). Figure 1.3 shows the temporal-vertical cross sections of the large-scale vertical velocity and zonal wind that are imposed in the model during the integration. Upward motions are dominant during most of integration period except that weak downward motions occur during 18–20 July 2006.

1.2.4 Experiment PSR

The data from NOAA/GDAS are used to calculate the forcing data for the model over a longitudinally oriented rectangular area of 108–116°E, 21–22°N over coastal areas along southern Guangdong and Guangxi Provinces and surrounding northern South China Sea in Experiment PSR. The model is imposed by large-scale vertical velocity, zonal wind (Fig. 1.4), and horizontal temperature and water vapor advections (not shown) and is integrated from 0200 LST 3 June to 0200 LST 8 June 2008 during the pre-summer heavy rainfall in experiment PSR. The imposed large-scale vertical velocity shows that upward motions increase from 3 June to 6 June with a maximum upward motion of 18 cm s^{-1} around 9 km in the late morning of 6 June. The upward motions decrease dramatically on 7 June. The lower-tropospheric westerly winds of 4–12 m s^{-1} are maintained during the rainfall event.

1.3 Comparison Between Simulations and Observations

1.3.1 Temperature and Specific Humidity

Gao and Li (2008b) compared the vertical profiles of simulated temperature and specific humidity in COARE with observations through the analysis of their differences in experiment COARE (Fig. 1.5). Compared to the observations, the simulations yield 1–2°C warmer upper troposphere and 1–2 g kg^{-1} more humid lower troposphere in December 1992 and 1–2°C colder mid and lower troposphere and 1 g kg^{-1} drier atmosphere in January 1993. The model tends to produce a cooling bias while the observed vertical temperature profile shows regular diurnal signals. The difference in specific humidity between the simulation and observation can be as high as 2–3 g kg^{-1} in the lower troposphere from 31 December 1992 to 3 January